



# Improvement of Pitting Corrosion Resistance and Anti-corrosion Performance of Aluminum 1200 by Eco-friendly Zr-based Conversion Coatings: Effect of Deposition Parameters

Seyed Mohammad Javad Yousefi Sharikabad<sup>1</sup> · Ramtin Hessam<sup>1</sup> · Hamed Aghili<sup>1</sup> · Sirus Javadpour<sup>1</sup>

Received: 21 November 2022 / Revised: 27 March 2023 / Accepted: 27 April 2023 / Published online: 16 May 2023  
© The Author(s), under exclusive licence to Springer Nature Switzerland AG 2023

## Abstract

Zr-based conversion coatings have received a lot of attention in recent years because of their green benefits, which offer nontoxic properties in comparison to conventional chromate and phosphate coatings. This study aims to investigate the effects of deposition parameters on the properties of Zr-based conversion coatings. The surface morphology, chemical composition, pitting corrosion resistance and corrosion performance of such coatings are studied using scanning electron microscopy (SEM), energy-dispersive X-ray spectroscopy (EDX), potentiodynamic polarization and salt spray techniques, respectively. Optical microscope and adherence test method are used to show the pits formed after potentiodynamic polarization and the adhesion of an organic coating to the samples. The SEM micrographs and EDX results revealed that increasing pH value,  $H_2ZrF_6$  concentration, deposition temperature and immersion time result in the formation of Zr-based conversion coating with unfavorable agglomerated areas, microcracks and non-uniformity of coating. The different experiments showed that superior pitting corrosion resistance coating could come from a bath with 100 mg/l hexafluorozirconic acid ( $H_2ZrF_6$ ), at the pH value of 4, the temperature of 25 °C and the immersion time of 3 min. Moreover, the adhesion of organic coating to coated Al 1200 is higher than uncoated Al 1200.

**Keywords** Al 1200 · Zr-based conversion coatings · Deposition parameters · Pitting corrosion

## 1 Introduction

Aluminum and its alloys have excellent corrosion resistance in marine, urban and industrial environments [1]. The 1xxx series, commercial aluminum alloys with 99% purity, possess excellent corrosion resistance compared to other aluminum alloys. The 1xxx series aluminum alloys due to their excellent corrosion resistance, high thermal conductivity,

and low density are used in various applications such as packaging industry, chemical equipment, kitchen utensils, tank car and truck bodies [2]. Among 1xxx series aluminum alloys, aluminum 1200 alloys have been widely used in the biomedical implants, automotive and electrical industries [2, 3]. These alloys are more susceptible to local corrosion due to the presence of a relatively high percentage of alloying elements (iron, silicon) in their crystal structure. The existence of these elements in their crystal structure leads to the formation of  $Al_6Fe$ ,  $Al_3Fe$  and  $Al_{12}Fe_3Si_2$  intermetallic particles that are preferential sites for pitting corrosion in these aluminum alloys [3]. One of the practical techniques to enhance the corrosion resistance of 1xxx series aluminum alloys is the deposition of conversion coatings on the surface of such alloys [4].

The surface properties of these alloys can be further improved through the application of various types of coatings, such as anodizing, painting, or conversion coatings. Anodizing is a commonly used surface treatment for aluminum alloys, which involves the formation of a protective oxide layer through an electrochemical process. Aghili et al.

✉ Seyed Mohammad Javad Yousefi Sharikabad  
smjyousefi@gmail.com

✉ Sirus Javadpour  
javadpor@shirazu.ac.ir

Ramtin Hessam  
ramtinhessam@gmail.com

Hamed Aghili  
hmd\_aghili@yahoo.com

<sup>1</sup> Department of Materials Science and Engineering,  
School of Engineering, Shiraz University, Zand Blvd.,  
Shiraz 7134851154, Iran

investigated the effect of various factors on the anodization process of 1xxx series aluminum alloys, such as the type of electrolyte, the anodizing voltage and surface preparation [5]. Painting is another common method used to protect the surface of alloys that can provide both decorative and protective functions [6]. Conversion coatings are also commonly used to improve the corrosion resistance and adhesion of subsequent coatings to enhance anti-corrosion behavior, mechanical properties, and biocompatibility [7].

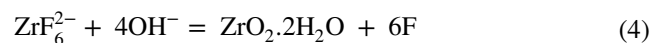
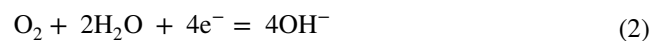
The conversion coating is applied on the surface of metals and alloys by chemical or electrochemical reaction between the metal and the solution [8–10]. Such coatings are used to improve corrosion resistance and facilitate adhesion between the painting and the substrate [8, 11]. Phosphate and chromate conversion coatings are the most common and familiar in different industries [12]. The adhesion between painting and the surface of ferrous alloys in the automotive industry is generally improved by phosphate conversion coating [8, 9]. The phosphating process is not a cost-effective method because it requires consuming a large amount of energy and removing sludge from the phosphating bath [8, 13]. On the other hand, the chromate conversion coatings that are typically applied on light metals play a crucial role in the pretreatment of aerospace products [8, 9]. The presence of  $\text{Cr}^{+6}$  in Cr-based pretreatment baths results in toxicity, so the production of chromate conversion coatings has been banned in different industries [13]. It has been several decades since considerable research has been conducted on the application of environmentally friendly and novel conversion coatings with the possibility of being applied at low temperature with high corrosion resistance and low cost to replace toxic and conventional conversion coatings [7, 8]. Other studies have focused on the development of environmentally friendly conversion coatings, such as those based on nanotechnology to reduce the use of hazardous chemicals [15]. Moreover, utilizing different kinds of ceramics nanomaterials coating, such as  $\text{Al}_2\text{O}_3$ ,  $\text{ZrO}_2$ , and  $\text{TiO}_2$  play a role in the improvement the mechanical and chemical properties of these coatings [16].

Previous research studies have focused on the introduction of new conversion coatings based on cerium [11–13, 19], lanthanum [21], vanadium [22], titanium [23, 24], magnesium [25] and zirconium [15, 16]. Among these coatings, the zirconium (Zr) conversion coating can be a reliable alternative to conventional conversion coatings, and has offered cost-effective coatings compared to the phosphate-based and chromate-based pretreatments [28].

Zirconia conversion coatings have been shown to provide superior corrosion protection compared to traditional conversion coatings [29]. Zirconia conversion coatings have been investigated as a promising alternative to traditional conversion coatings for aluminum alloys. In particular, zirconia conversion coatings have shown excellent corrosion

resistance and adhesion properties on aluminum 1200, which is a widely used aluminum alloy in various industries. One such application is in the automotive industry, where zirconia conversion coatings have been shown to provide superior corrosion protection compared to traditional conversion coatings. In addition, zirconia coatings have been investigated for their potential use as a surface treatment for biomedical implants due to their biocompatibility and the ability to improve the osseointegration of implants [30]. Furthermore, zirconia conversion coatings have been studied for their potential use in the aerospace industry to protect aluminum alloys from corrosion in harsh environments [29].

The proposed reactions that result in the deposition of Zr-based conversion coatings are:



where, aggressive  $\text{H}^+$  and  $\text{F}^-$  ions dissolve the aluminum oxide thin film on aluminum to prepare the substrate for the initial step of deposition of a conversion coating. On the other hand, the reduction of  $\text{O}_2$  and the evolution of  $\text{H}_2$  take place in the cathodic areas of the substrate so that the amount of  $\text{OH}^-$  increases. This phenomenon (increasing pH) leads to the hydrolysis of  $\text{ZrF}_6^{2-}$  which pave the way for the deposition of  $\text{ZrO}_2 \cdot 2\text{H}_2\text{O}$  films [31].

Among the recent studies conducted on the deposition of Zr-based conversion coatings, Hamdy et al. have investigated the effect of zirconate concentration on the uniform corrosion behavior of Zr-based conversion coatings that were applied on magnesium AZ31D alloy. They have demonstrated that using 20 g/l zirconate solution exhibited the best corrosion resistance due to the minimization of active sites and rejection of  $\text{Cl}^-$  ions on the surface [32]. H. Eivaz Mohammadloo et al. have shown that the processing parameters of Zr-based conversion coatings such as immersion time, solution pH and temperature can influence electrochemical and morphological properties of Zr-based conversion coatings deposited on cold-rolled steel substrates [33]. The uniform corrosion behavior of Zr-based conversion coatings applied on mild carbon steel (st 37) at various pH values and hexafluorozirconic concentrations has been investigated by H.R. Asemiani et al. They revealed that more uniform coatings with the highest corrosion resistance could be applied by the bath containing 0.01 M hexafluorozirconic ( $\text{H}_2\text{ZrF}_6$ ) concentration with pH=4.5 [34]. Among the different processing parameters used to deposit conversion

coatings, zirconate concentration and pH value could be mentioned as the parameters that are more effective for the deposition of such coatings by this method [24–26]. Controlling the concentration of zirconate exerts a direct effect on the amount of Zr within the deposited coatings influencing the corrosion resistance of coatings. In fact, the formation of Zr-rich film at the surface of substrate can act as a barrier to oxygen diffusion to the metal surface which results in improving the corrosion performance of such coatings [25]. Using higher pH values also affects the rate of conversion coating deposition process [33].

Although some researchers have investigated the deposition of Zr-based conversion coatings and their uniform corrosion behaviors, there are not enough research studies on the influence of deposition parameters on the local corrosion of such coatings. The main aim of this research is to study the pitting corrosion of Zr conversion coatings deposited on 1200 aluminum substrates because such alloys are more exposed to local corrosion specially pitting corrosion. Moreover, chemical composition, morphology, anti-corrosion performance and adherence of Zr-based conversion coatings that were deposited on the surface of Aluminum 1200 alloy samples under various experimental conditions. commercially pure aluminum alloys are more exposed to pitting corrosion, the present study aims to investigate the effects of deposition parameters on the

50%wt Hexafluorozirconic ( $H_2ZrF_6$ ) acid solution. To investigate the effects of processing parameters on the chemical composition, morphology, roughness value and pitting corrosion resistance and anticorrosion behavior of zirconium conversion coatings, the bath pH values,  $H_2ZrF_6$  concentrations, deposition temperatures, and immersion times used in this work are shown in Table 1.

A scanning electron microscopy instrument (TESCAN-Model Vega 3) equipped with an energy-dispersive X-ray spectrum (Model RONTEC, QUANTAX Software) was used to investigate morphologies and micro area compositions of coatings. The SEM analyses for all samples were performed by the SEM magnification and SEM voltage of  $2000\times$  and 20 kV for all samples, respectively. Average surface roughness ( $R_a$ ) values were measured using the Mitutoyo Surftest 201 device with a distance that a stylus moves at 0.9 cm (diameter of samples). The potentiodynamic polarization test was carried out by  $\mu$  AUTOLAB (Type III) in 3.5 wt.% NaCl solution to investigate the pitting corrosion of deposited coatings using a conventional three-electrode cell equipped with the specimen, Ag/AgCl and Pt as a working electrode, reference electrode and counter electrode, respectively. In all polarization tests, the specimens were polarized from  $-1200$  to  $-300$  mV with respect to open circuit potential ( $V_{OCP}$ ) with a potential scan rate of 1 mV/s [35, 36]. The organic coating applied on samples by doctor blade coating machine and the anti-corrosion performance of such coatings were investigated by the salt spray test based on ASTM B117 standard (at  $30^\circ C$  and exposed to NaCl 5 wt.% salt solution spray). All samples were coated with Alkyd organic painting and they were placed in a salt spray cabin SF/MP1000 for 500 h. ImageJ software was used to estimate the percentage of corroded area by salt spray experiment. The adherence test method was performed by Elcometer 107 device to investigate the adherence of the organic coating based on ASTM D3359-02 standard.

## 2 Material and Methods

Al 1200 rods ( $d=0.9$  cm) were abraded to 3000 grit with SiC polishing paper and cleaned with acetone to remove scratches and contaminants on samples. Then, alkaline and acid etching were carried out in NaOH (5%w/w at  $50^\circ C$ ) solution and nitric acid (50%v/v at  $25^\circ C$ ), respectively, to clean samples from oxide layers. In the final step, the samples were immediately immersed in the bath containing

**Table 1** The operating parameters employed and their related sample coding for the design of experiments

Deposition parameters	Value	Sample code	Variable directions and design roots		
Concentration of $H_2ZrF_6$ (mg/l)	50,100,200	4/100/25/1	4/50/25/3	4/100/15/3	
pH	3,4,5	3/100/25/3	4/100/25/3	5/100/25/3	
Temperature ( $^\circ C$ )	15,25,35	4/100/35/3	4/200/25/3	4/100/25/5	
Immersion time (min)	1,3,5	Reference code: pH/C/T/t Root: Sequence of experiment to find optimal sample			

### 3 Results and Discussion

#### 3.1 Microstructural Analysis

Figure 1 illustrates the top-view SEM micrograph and EDX analysis results of the Al 1200 substrate after the polishing process. Some white particles on the micrograph indicate the slight dissolution of the substrate. Regarding the results of EDX, these particles are composed of iron and silicon elements which can act as cathodic active sites and pitting corrosion initiation [37].

The SEM micrographs and EDX results attributed to the coatings prepared at various pH values are provided in Fig. 2. As seen, the surface of the film synthesized at pH = 3 (3/100/25/3) did not change compared to that of the substrate (untreated sample); moreover, the EDX analysis shows the presence of 0.31% zirconium in the coating applied under this experimental condition.

Based on the Pourbaix diagram attributed to aluminum, zirconium, fluorine, and zirconium-fluorine (shown in Fig. 3), zirconium and aluminum are placed in the corrosion zone at pH = 3 as well as the possibility of hydrofluoric acid (HF) formation increases which prevents the formation of a uniform zirconium coating [38]. By raising the pH value to 5 (sample 5/100/25/3), the amount of zirconium in the coating increases to 9.47 wt.% and the formation of the coatings becomes thermodynamically favorable (Fig. 3). In terms of kinetic aspect, the coating deposited at pH = 5 experienced a higher deposition rate as a result of increasing the reaction rate given in Eq. (4).

Thus, the high deposition rate leads to the formation of more porous and non-uniform zirconium coatings on the substrate. This observation is consistent with previous research studies performed on the effect of pH value on the formation of Zr-based conversion coatings [33, 39].

Figure 4 shows the effect of  $H_2ZrF_6$  concentration on SEM micrographs and EDX results of coatings. As seen, using the bath containing the higher  $H_2ZrF_6$  concentration resulted in the formation of coatings with higher percentage of Zr. Moreover, the agglomerated particles and cracks were observed in the SEM micrograph of the coating applied in the bath containing the highest  $H_2ZrF_6$  concentration (200 mg/l) due to the increase in the rate of deposition and the number of destructive fluoride ions under such experimental conditions. Some previous studies have demonstrated that the increase in the concentration of destructive fluoride ions causes the formation of cracks in Zr-based conversion coatings [32]. Similar behavior has been reported in the case of these coatings applied on the steel substrate at various concentrations of  $H_2ZrF_6$  [13, 33].

The SEM micrographs and EDX results attributed to the coatings deposited at different bath temperatures are provided in Fig. 5. As seen, the rise of the bath temperature from 15 to 35 °C led to an increase in the weight percentage of Zr in the coatings from 0.87 wt.% to 8.59 wt.%. Moreover, non-uniform patches with local dissolution areas of the coating (black areas) were observed on the surface of the coating applied at the temperature of 35 °C (4/100/35/3). In terms of thermodynamic aspect, as temperature increases (up to 423 K), the area of zirconium oxide formation in the Pourbaix diagram decreases [40].

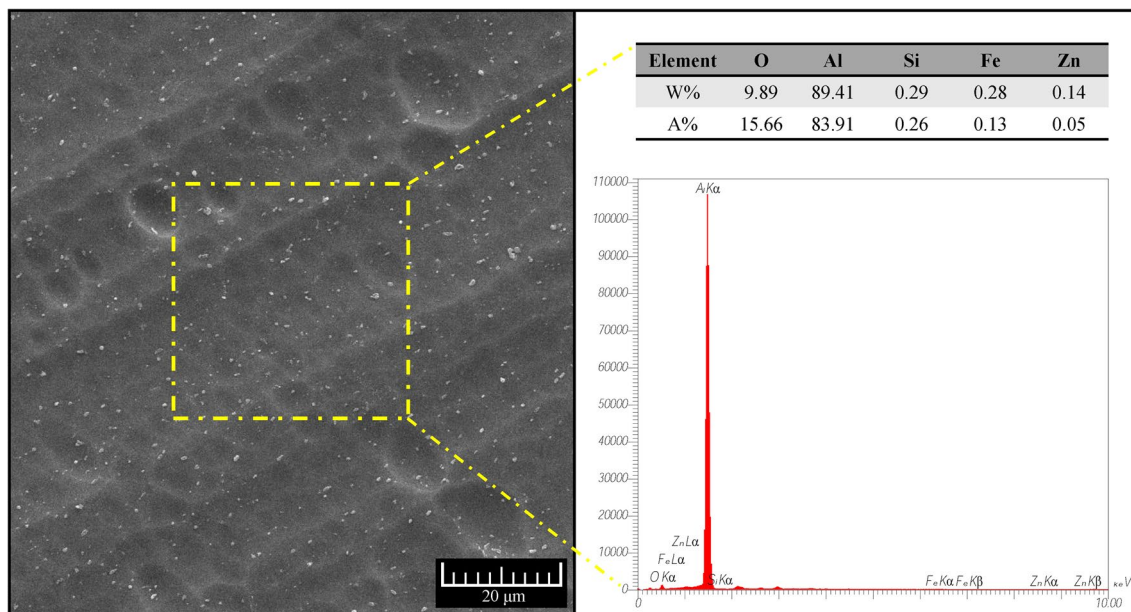
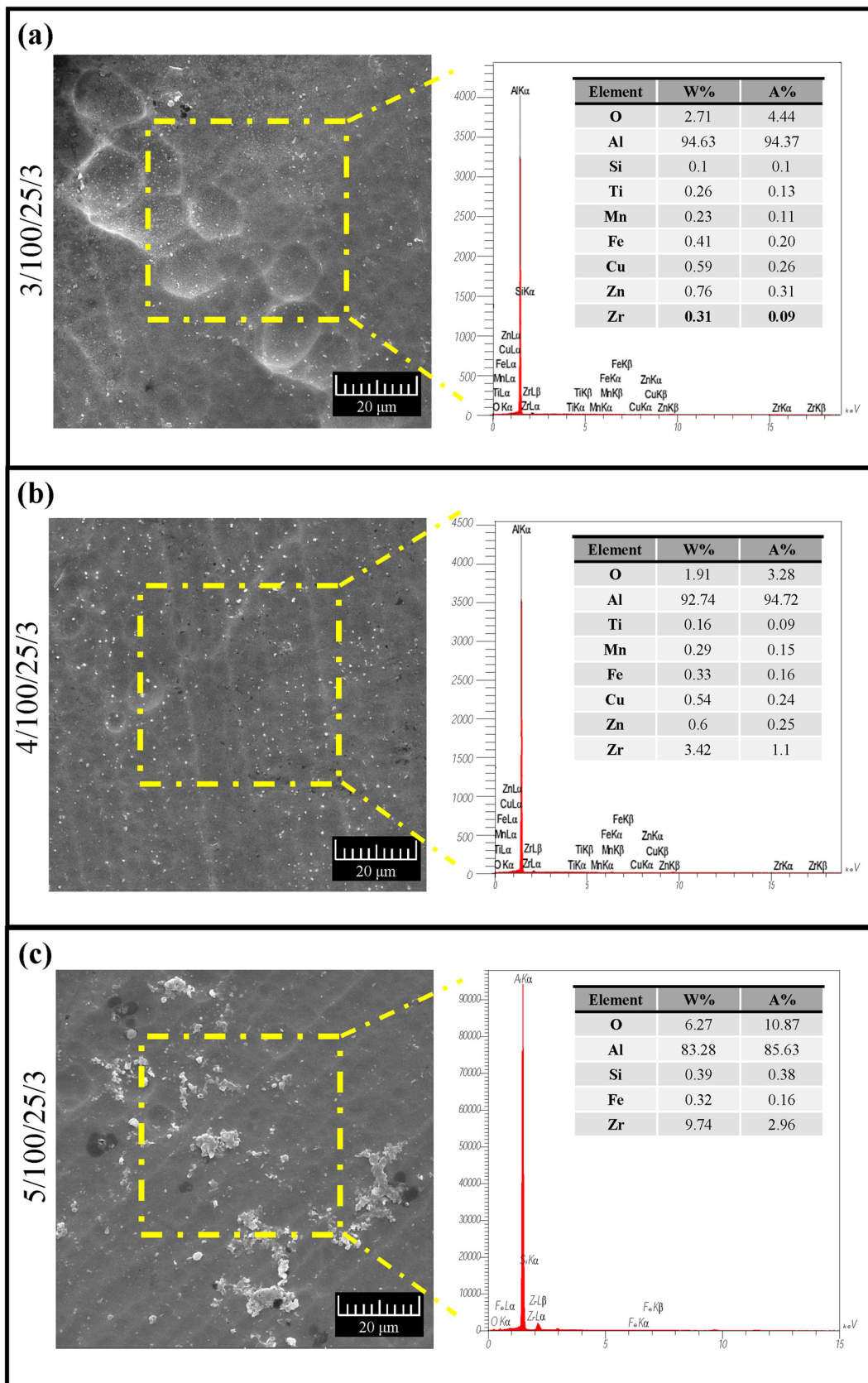


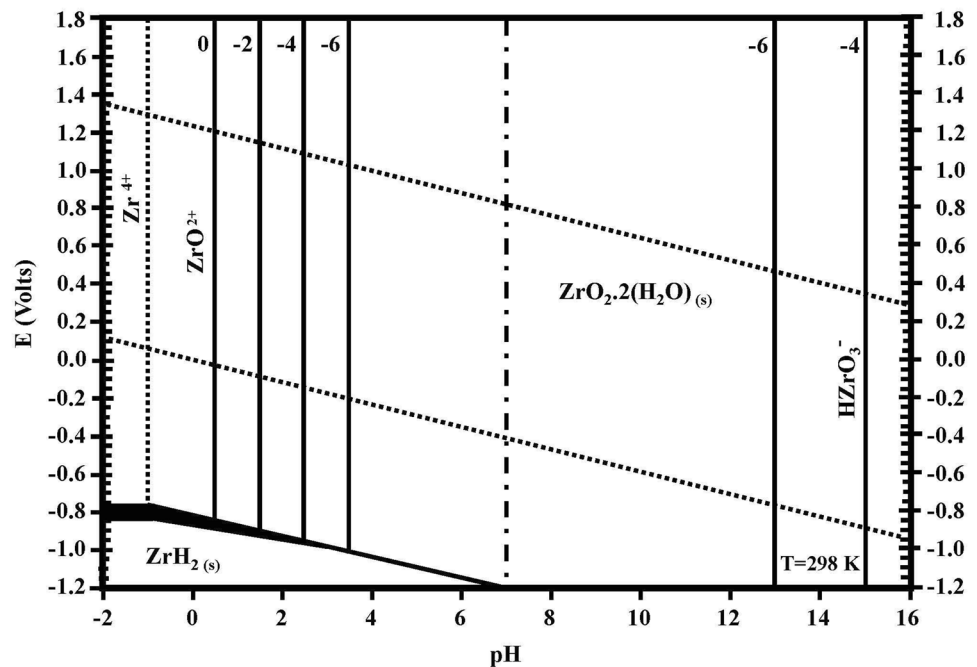
Fig. 1 a SEM image and b EDS analysis from the surface of the Al bare substrate





**Fig. 2** SEM images and EDS analysis from the surface of conversion coatings applied at various pH values of **a** 3, **b** 4 and **c** 5 in the bath containing 100 mg/l of  $H_2ZrF_6$  at  $T=25\text{ }^\circ\text{C}$  and  $t=3\text{ min}$

**Fig. 3** The Pourbaix diagram of zirconium in water at 298 K [40]



The effect of temperature on the rate of reactions that take place in the bath can be described by the following Eq. (5):

$$L = (Dt)^{1/2} \quad (5)$$

in which,  $L$  is the penetration length of the ions in the bath,  $t$  is the immersion time, and  $D$  is the diffusion coefficient of ions in the bath which has a direct relation with temperature. Thus, using higher bath temperatures leads to enhancing the diffusion coefficient of ions that increases the reaction rate in the bath [41]. In the case of the coating deposited at 35 °C, the rate of reactions (From Eq. (1) to Eq. (4)) increases, however, the condition of coating dissolution is more thermodynamically favorable. This observation is consistent with the results that have been reported for Zr-based conversion coatings applied using various temperatures on cold-rolled and hot-dip galvanized steel substrates [13, 33].

Figure 6 illustrates the SEM micrographs and the EDX results of the coatings applied at various immersion times. As can be seen, the percentage of Zr in the coatings increased to 9.49 wt.% using the longest immersion time (5 min). According to SEM images, the uniform coatings with a suitable distribution on the surface were deposited by immersing at 3 min. When the deposition of coatings performs for up to 3 min, the coatings microstructure changes to a massive and porous structure; moreover, cracks and local dissolution areas (black areas) could be seen on the micrograph of coatings applied under this experimental condition. Based on Eq. (5), the immersion time also can affect the ion diffusion length. The coating deposited at the lowest immersion time (1 min), not only experiences the small ion

diffusion but also the largest amount of time is spent dissolving the surface oxide layers (according to Eq. (5)). As a result, the substrate cannot be covered with a uniform and suitable coating at this deposition condition [39]. However, there are some cracks observed on the surface of the coating applied by the immersion time of 5 min (4/100/25/5) due to the creation of internal stresses in the structure of the coating [28].

### 3.2 Roughness Test

Figure 7 compares the surface roughness value of the untreated sample and the deposited Zr-based coatings. As seen, the Zr-based coatings exhibited higher surface roughness values than the untreated sample. In addition, increasing  $H_2ZrF_6$  concentration in the bath, immersion time, bath pH and temperature led to the formation of coatings with higher roughness values. The increase in the roughness value of conversion coatings deposited in more bath concentrated and higher bath pH conditions is attributed to the formation of micro-agglomerates (Figs. 2 and 4), while the formation of dissolved area and microcracks on the surface of conversion coatings deposited at higher bath temperature and longer duration (Figs. 5 and 6) resulted in the formation of such coatings with higher roughness values.

### 3.3 Potentiodynamic Polarization Test

The potentiodynamic polarization curves for the untreated sample and Zr-based coatings are shown in Fig. 8. Electrochemical data including  $E_{\text{corr}}$  (corrosion potential),  $E_{\text{pit}}$

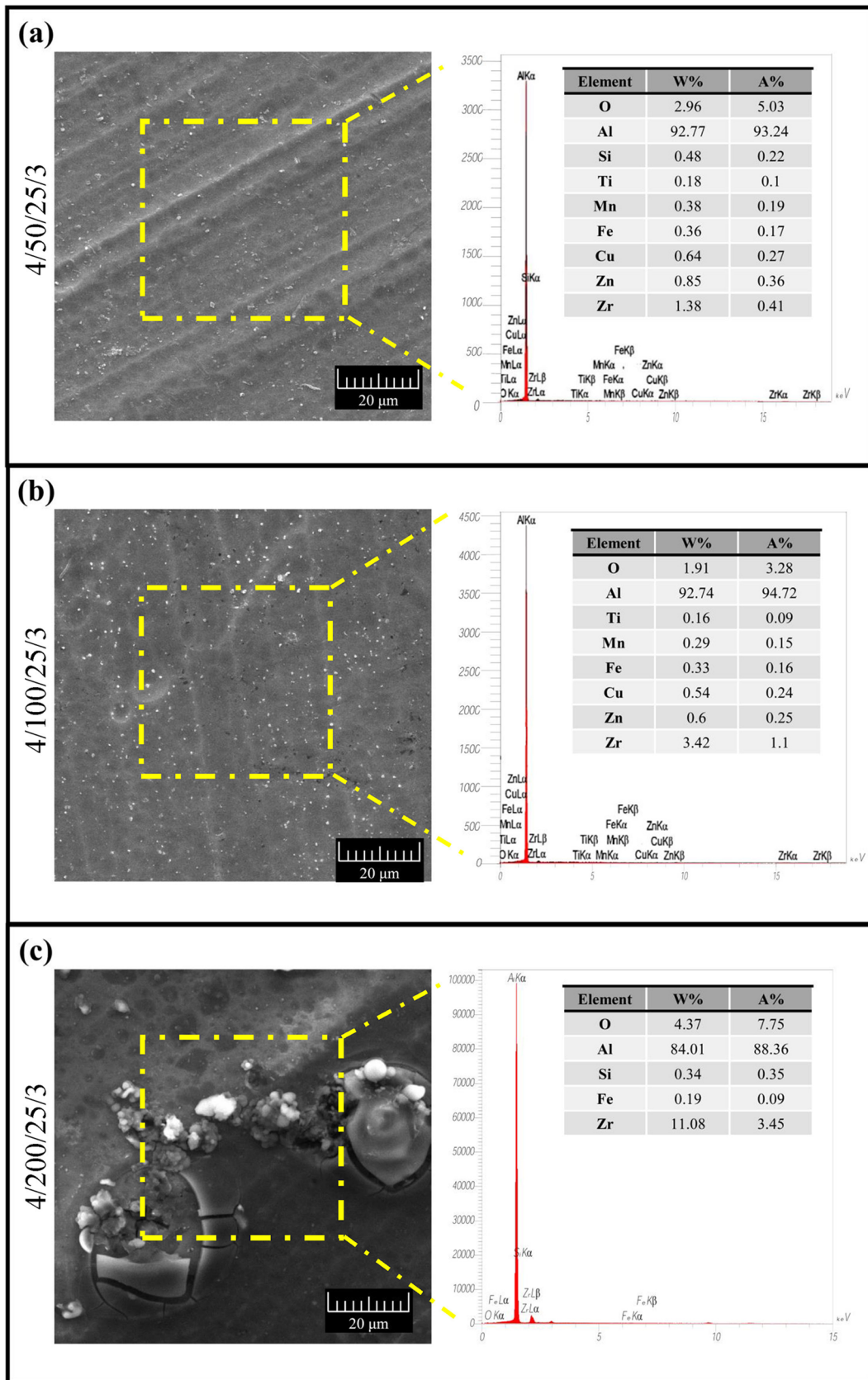


**Fig. 4** SEM micrographs and EDS analysis from the surface of conversion coating applied in the bath containing different concentrations of  $H_2ZrF_6$ : **a** 50 mg/l, **b** 100 mg/l and **c** 200 mg/l, at pH=4,  $T=25\text{ }^\circ\text{C}$  and  $t=3\text{ min}$

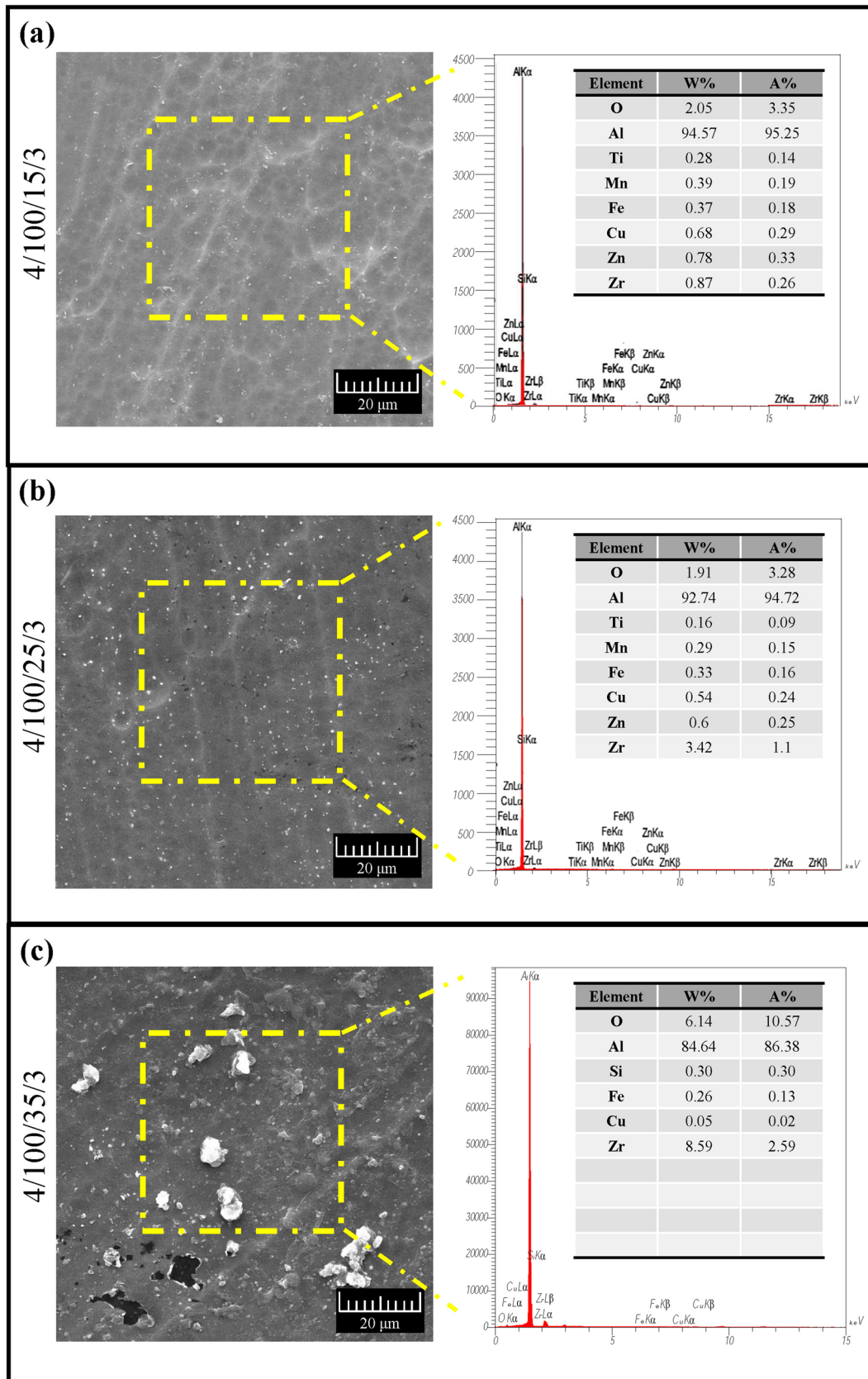


**Fig. 5** SEM images and EDS analysis from the surface of conversion coating formed in the bath containing 100 mg/l of  $H_2ZrF_6$ , at  $t=3$  min, pH=4 and different bath temperatures: **a** 15 °C, **b** 25 °C and **c** 35 °C



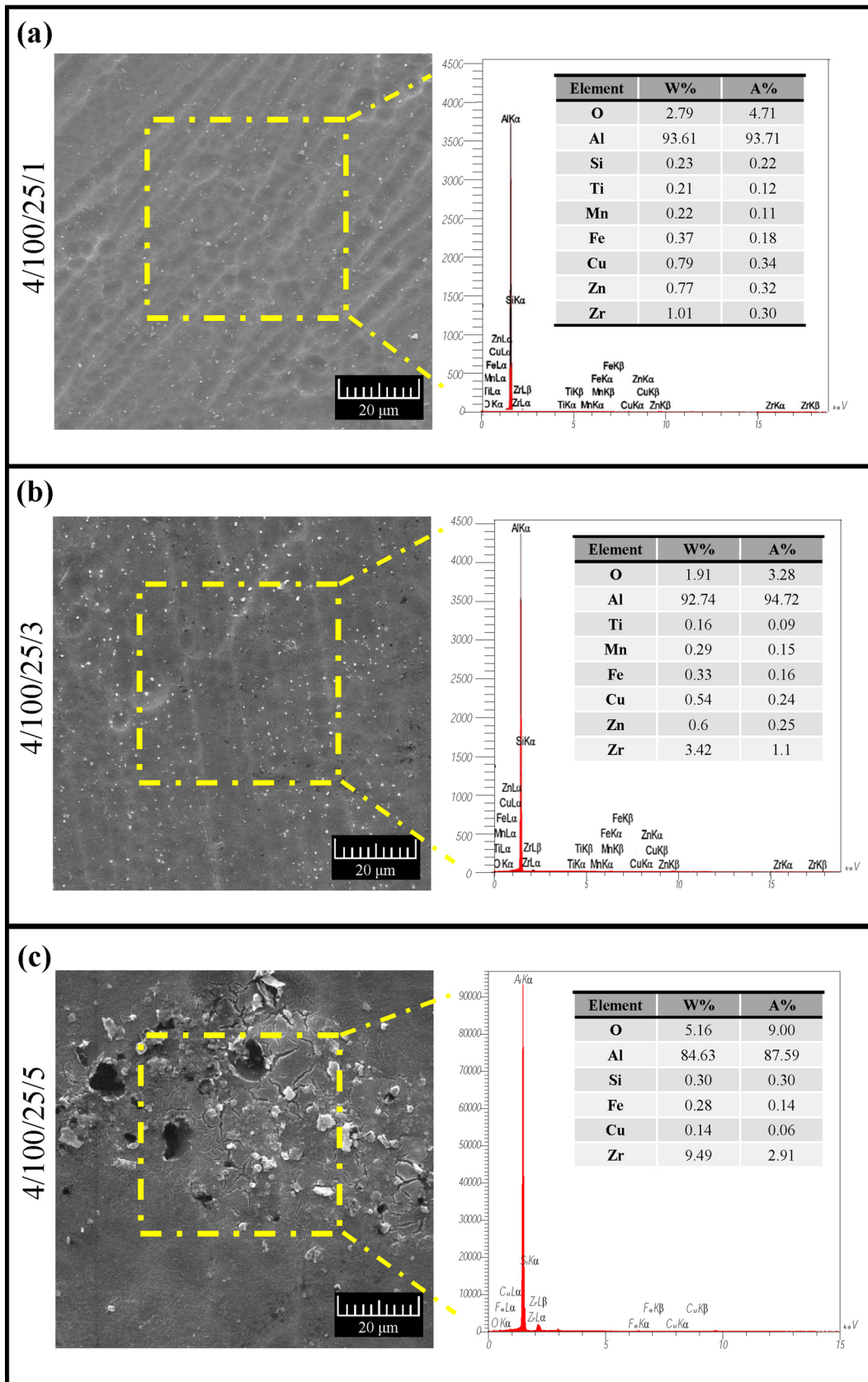


**Fig. 6** SEM images and EDS analysis from the surface of the conversion coatings applied in the bath containing 100 mg/l of  $H_2ZrF_6$ , at pH=4,  $T=25\text{ }^\circ\text{C}$  and different immersion times: **a** 1 min, **b** 3 min and **c** 5 min

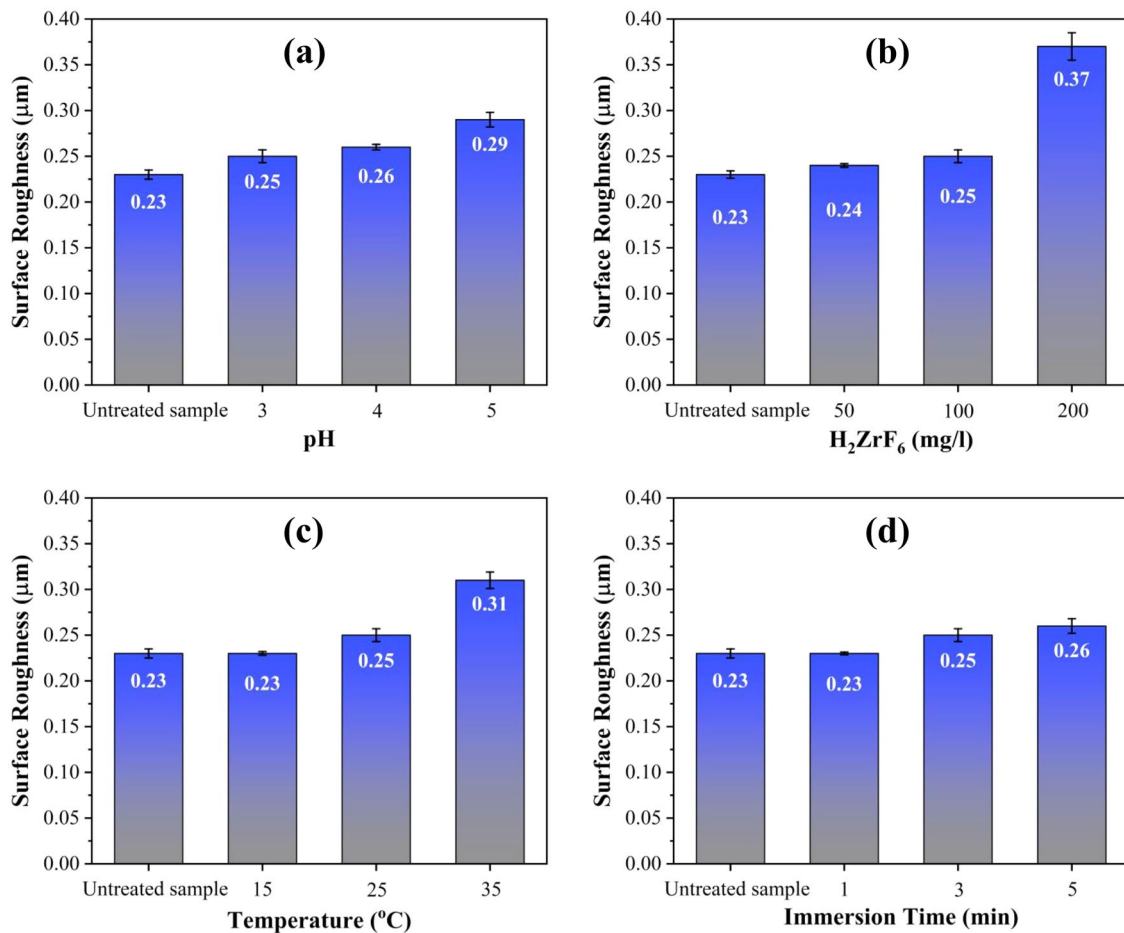


**Fig. 7** Surface roughness values of the bare sample and Zr conversion coatings were applied by different **a** pH values, **b** H<sub>2</sub>ZrF<sub>6</sub> concentrations, **c** bath temperatures and **d** immersion times

(pitting or breakdown potential),  $E_{\text{pit}} - E_{\text{corr}}$  (pitting corrosion resistance) and C.R. (corrosion rate) were extracted using NOVA software and reported in Table 2. As seen, the untreated sample showed the lowest pitting corrosion resistance (smaller difference between  $E_{\text{pit}}$  and  $E_{\text{corr}}$ ) compared to the deposited Zr-based conversion coatings. This result would be related to eliminating the effect of cathodic areas (intermetallic areas) on the aluminum substrate [33] and minimizing half-cathodic reactions during corrosion, which can enhance uniform corrosion resistance by the deposition of such coatings [42].

In addition, the pitting corrosion resistance of the coatings deposited at pH = 4 is higher than those formed at the pH values of 3 and 5 as the coatings deposited at such pH values are not uniform and have more porosities which provide nucleation sites for pitting corrosion [43]. The pitting corrosion resistance of Zr-based conversion coatings is improved by increasing the concentration of H<sub>2</sub>ZrF<sub>6</sub> in the bath to 100 mg/l because of the formation of a uniform coating under this experimental condition. However, the

coating deposited in a bath containing 200 mg/l of H<sub>2</sub>ZrF<sub>6</sub> exhibits lower resistance against pitting corrosion than the untreated sample. This result could be related to the formation of cracks and agglomerated particles on the surface of the coating deposited in the bath containing 200 mg/l of H<sub>2</sub>ZrF<sub>6</sub> (4/200/25/3) [44]. Zr-based coatings deposited at 15 °C (4/100/15/3) and 25 °C (4/100/25/3) showed higher pitting resistance than coatings synthesized at the higher bath temperature (35 °C) due to the deposition of uniform ones without having porosity at lower bath temperatures [43]. It is crystal clear that the Zr coatings deposited at 3 min had better pitting corrosion resistance compared to those prepared at other immersion periods. As mentioned for other influential parameters, in this case, uniform distribution of the coating over the intermetallic areas can increase the resistance against pitting corrosion. There is no significant difference in the pitting corrosion resistance of the uncoated sample and the coating deposited at 1 min because most of the immersion time is spent on the dissolution of the oxide layers on the surface. Thus, the suitable coating is not

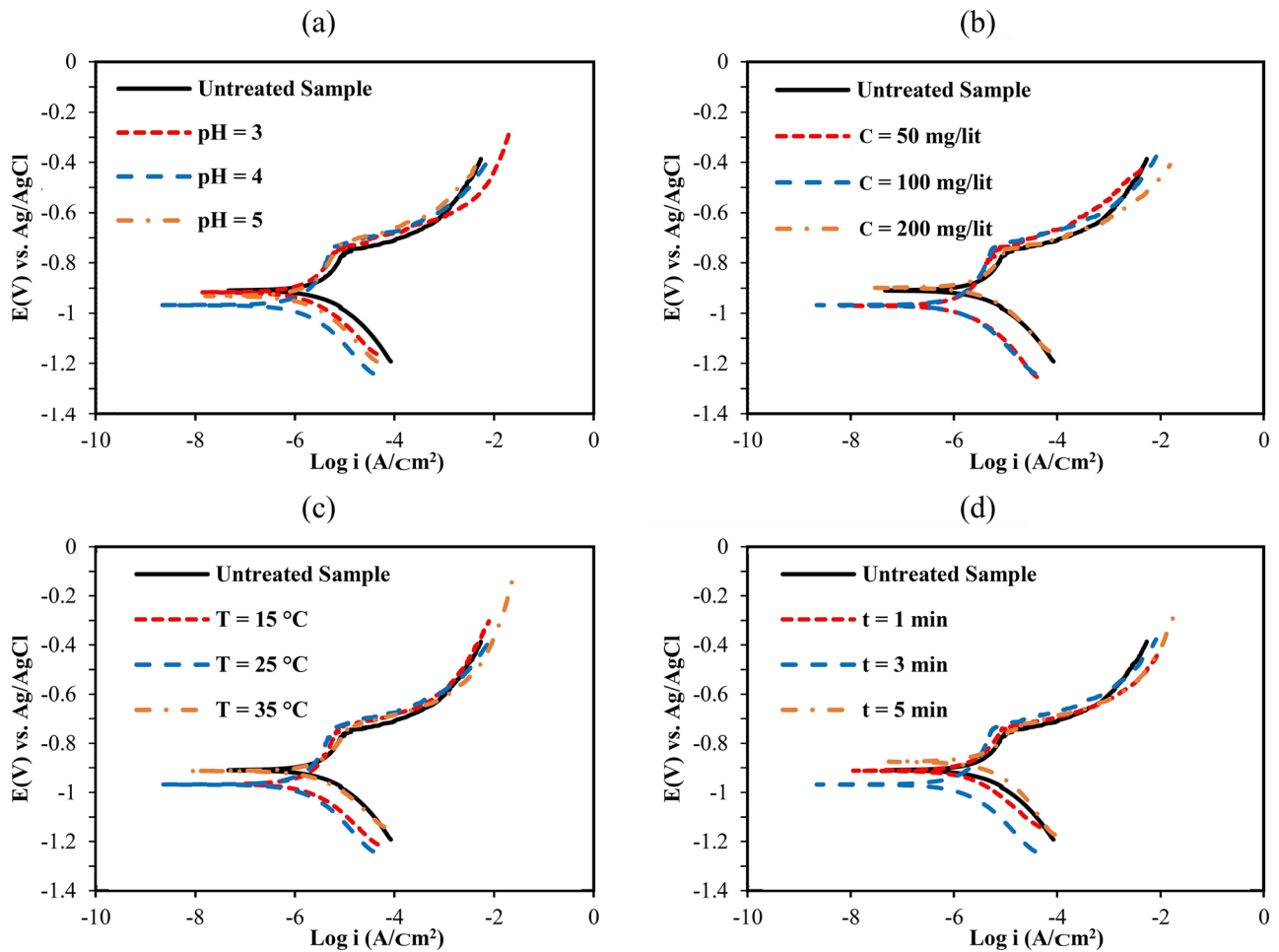


**Fig. 8** Potentiodynamic polarization plots of the bare Al and conversion coatings were applied by different **a** pH values, **b** H<sub>2</sub>ZrF<sub>6</sub> concentrations, **c** bath temperatures and **d** immersion times

**Table 2** Electrochemical parameters extracted from potentiodynamic polarization plots attributed to the bare Al and conversion coatings were applied by different (a) pH values, (b) H<sub>2</sub>ZrF<sub>6</sub> concentrations, (c) bath temperatures and (d) immersion times

		Sample	E <sub>corr</sub> (V)	E <sub>pit</sub> (V)	R <sub>pit</sub> (V)	C.R (mm/year)
		Untreated	-0.910	-0.767	0.143	0.145
(a)	pH	3/100/25/3	-0.916	-0.750	0.166	0.084
		4/100/25/3	-0.968	-0.744	0.224	0.063
		5/100/25/3	-0.931	-0.727	0.204	0.082
(b)	Zr concentration	4/50/25/3	-0.970	-0.758	0.212	0.068
		4/100/25/3	-0.968	-0.744	0.224	0.063
		4/200/25/3	-0.898	-0.762	0.136	0.114
(c)	Temperature	4/100/15/3	-0.965	-0.748	0.219	0.088
		4/100/25/3	-0.968	-0.744	0.224	0.063
		4/100/35/3	-0.912	-0.753	0.159	0.147
(d)	Time	4/100/25/1	<i>t</i> = 1 min	-0.744	0.168	0.091
		4/100/25/3	<i>t</i> = 3 min	-0.744	0.224	0.063
		4/100/25/5	<i>t</i> = 5 min	-0.754	0.121	0.150

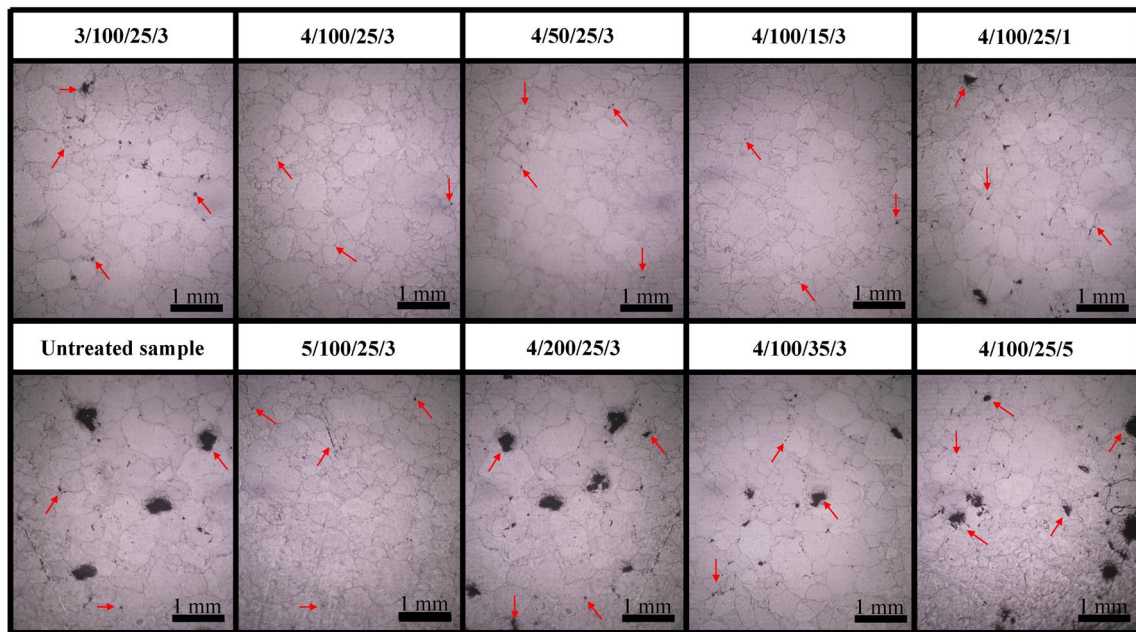


Fig. 9 Optical Microscopy (OM) images from the surface of the samples after potentiodynamic polarization analysis

Sample \ Hours	0	200	500	Corroded Area (%)	Sample \ Hours	0	200	500	Corroded Area (%)
Untreated				15.57	pH= 4 t= 1 min T= 25 °C C= 100mg/l				9.26
pH= 3 t= 3 min T= 25 °C C= 100mg/l				6.63	pH= 4 t= 5 min T= 25 °C C= 100mg/l				7.33
pH= 4 t= 3 min T= 25 °C C= 100mg/l				4.76	pH= 4 t= 3 min T= 15 °C C= 100mg/l				8.87
pH= 5 t= 3 min T= 25 °C C= 100mg/l				9.84	pH= 4 t= 3 min T= 35 °C C= 100mg/l				10.23
pH= 4 t= 3 min T= 25 °C C= 50mg/l				8.63	pH= 4 t= 3 min T= 25 °C C= 200/l				9.87

Fig. 10 Images from the surface of organic coating samples with and without Zr conversion coating pretreatment after different exposure times of salt spray tests

formed in areas that are exposed to corrosion. On the other hand, the pitting corrosion resistance of Zr-based conversion coatings deposited at longer immersion times (5 min) is lower than that of the untreated sample due to the formation

of agglomerated particles, small cracks and local dissolution areas on the surface of the coatings [44].

Figure 9 shows Optical Microscopy (OM) images from the surface of the samples after performing potentiodynamic polarization analysis. As seen, large pits can be observed



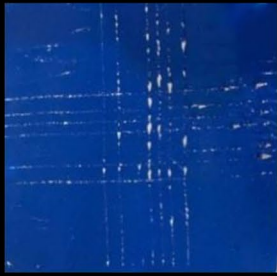


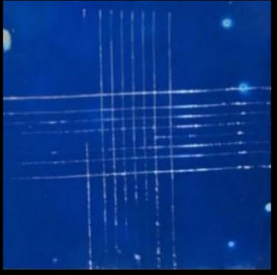
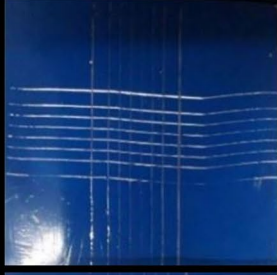
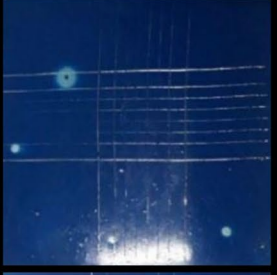
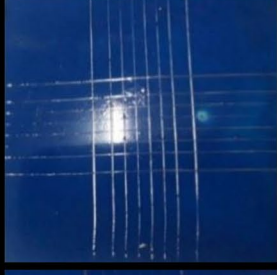
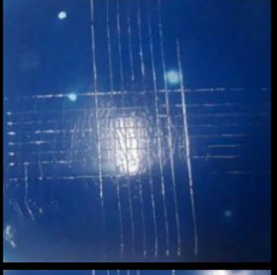


Samples	Adhesion Area	Samples	Adhesion Area
pH= 4 t= 1 min T= 25 °C C= 100mg/l		pH= 4 t= 1 min T= 25 °C C= 100mg/l	
pH= 3 t= 3 min T= 25 °C C= 100mg/l		pH= 4 t= 5 min T= 25 °C C= 100mg/l	
pH= 4 t= 3 min T= 25 °C C= 100mg/l		pH= 4 t= 3 min T= 15 °C C= 100mg/l	
pH= 5 t= 3 min T= 25 °C C= 100mg/l		pH= 4 t= 3 min T= 35 °C C= 100mg/l	
pH= 4 t= 3 min T= 25 °C C= 50mg/l		pH= 4 t= 3 min T= 25 °C C= 200/l	

Fig. 11 The adherence test results attributed to the organic coating applied on untreated and treated samples

in untreated sample while the number of pits decreases for the samples coated by Zr conversion coating. Moreover, the number and size of pits decreased for the samples that have

higher pitting corrosion resistance so that limited number of small pits were observed for sample 4/100/25/3 which possesses excellent pitting corrosion resistance.

### 3.4 Salt Spray Test

Figure 10 illustrates the images captured from the organic coating applied on samples after 200 and 500 h and the estimated percentage of area corroded by the salt spray experiment. As seen, a smaller percentage of corroded area was seen on the surface of coated samples (with a range of 4.76–10.23%) compared to the uncoated sample (15.57%). This result would be attributed to the better adhesion of the organic coatings to the conversion ones. The deposition of conversion coatings on metals can lead to physical and chemical changes on their surfaces so that cathodic reactions cannot easily occur in the cathodic areas. As a result, the Zr-coated surfaces show better resistance against cathodic reactions during the movement of corrosive elements to the interface of substrate and coating [34]. Moreover, the sample 4/100/25/3 showed better resistance in salt spray analysis because the coating obtained using this experimental condition was free of any agglomerated areas, micro-cracks and possessed highest pitting corrosion resistance. This observation is consistent with previously reported research studies [34].

### 3.5 Adhesion Test

The adherence test pictures and the percent of detachment area (that was estimated based on ASTM D-3359–02) for all samples are shown in Fig. 11. As seen, the test area of the untreated sample coated with organic coating demonstrates the highest detachment (5–15%) of the organic coating while the samples that were treated with zirconium conversion coating exhibit no detachment. This result would be related to the combination of Zr with unpaired dienes (that exist in alkyd painting) which leads to the formation of an organic complex and previous research studies have shown that this organic complex can increase the adherence of organic paintings coated on different substrates [34, 45, 46].

## 4 Conclusion

In this study, Zr-based conversion coatings were applied on aluminum 1200 under various deposition conditions where:

- Increasing the pH value, immersion times,  $H_2ZrF_6$  concentrations, and deposition temperatures increased the amount of Zr in the coatings. However, these experimental conditions resulted in the formation of coatings with larger agglomerated areas, more micro-cracks, and higher roughness values.

- Samples 4/100/25/5 and 4/100/25/3 had the lowest and highest pitting corrosion resistance, respectively.
- Sample 4/100/25/3 with the corroded area of 4.76% showed the best anti-corrosion performance in salt spray experiment.
- The adhesion of organic coating to all Zr coated substrates was higher than the untreated sample.

**Author Contributions** SMJYS and HA: Material preparation, data collection and analysis were performed. RH: The first draft of the manuscript was written and SJ: the review of the manuscript was performed. All authors commented on previous versions of the manuscript.

**Funding** This research has been funded by Shiraz University.

**Data Availability** Not applicable.

### Declarations

**Conflict of interest** The authors have no conflicts of interest to declare.

## References

1. Peng C, Liu Y-W, Guo M-X, Tian-zhen Gu, Wang C, Wang Z-Y, Cheng SUN (2022) Corrosion and pitting behavior of pure aluminum 1060 exposed to Nansha Islands tropical marine atmosphere. *Trans Nonferrous Met Soc China* 32:448–460. [https://doi.org/10.1016/S1003-6326\(22\)65806-0](https://doi.org/10.1016/S1003-6326(22)65806-0)
2. Morshed-Behbahani K, Najafisayar P, Hessam R, Zakerin N (2020) Characterization of Anodic Films Produced on Anodized AA1050 Aluminum Alloy: Effect of Bio-additive. *Metall Mater Trans A Phys Metall Mater Sci* 51:5475–5483. <https://doi.org/10.1007/s11661-020-05957-0>
3. Witkowska M, Thompson GE, Hashimoto T, Koroleva E (2013) Assessment of the surface reactivity of AA1050 aluminium alloy. *Surf Interface Anal* 45:1585–1589. <https://doi.org/10.1002/sia.5271>
4. Sababi M, Terryn H, Mol JMC (2017) The influence of a Zr-based conversion treatment on interfacial bonding strength and stability of epoxy coated carbon steel. *Prog Org Coat* 105:29–36. <https://doi.org/10.1016/j.porgcoat.2016.11.016>
5. Aghili H, Hashemi B, Bahrololoom ME, Jahromi SAJ (2019) Fabrication and characterization of nanoporous anodic alumina membrane using commercial pure aluminium to remove Coliform bacteria from wastewater. *Process Appl Ceram* 13:235–243. <https://doi.org/10.2298/PAC1903235A>
6. McMahan ME, Kammrath BW, Bender L (2023) Automotive Paint. *Encycl Forensic Sci*. Elsevier, Amsterdam
7. Kannan S, Madhu K, Nallaiyan R (2022) Formulation of magnesium conversion coating with herbal extracts for biomedical applications. *J Bio- Tribo-Corros* 8:114. <https://doi.org/10.1007/s40735-022-00715-8>
8. Eivaz Mohammadloo H, Sarabi AA (2016) Titanium composite conversion coating formation on CRS In the presence of Mo and Ni ions: Electrochemical and microstructure characterizations. *Appl Surf Sci* 387:252–259. <https://doi.org/10.1016/j.apsusc.2016.06.095>

9. Ogle K, Buchheit RG (2007) Conversion Coatings Encyclopedia of Electrochemistry. In: Bard MSAJ (ed) Encycl Electrochem. Wiley, Weinheim
10. Ling-yun AN, Ying MA, Xiao-xu YAN, Sheng WANG, Zhan-ying WANG (2020) Effects of electrical parameters and their interactions on plasma electrolytic oxidation coatings on aluminum substrates. *Trans Nonferrous Met Soc China* 30:883–895
11. Twite RL, Bierwagen GP (1998) Review of alternatives to chromate for corrosion protection of aluminum aerospace alloys. *Prog Org Coat* 33:91–100. [https://doi.org/10.1016/S0300-9440\(98\)00015-0](https://doi.org/10.1016/S0300-9440(98)00015-0)
12. Kim M, Brewer LN, Kubacki GW (2023) Microstructure and corrosion resistance of chromate conversion coating on cold sprayed aluminum alloy 2024. *Surf. Coatings Technol.* 460:129423. <https://doi.org/10.1016/J.SURFCOAT.2023.129423>
13. Mousavifard SM, Attar MM, Ghanbari A, Dadgar M (2015) Application of artificial neural network and adaptive neuro-fuzzy inference system to investigate corrosion rate of zirconium-based nano-ceramic layer on galvanized steel in 3.5% NaCl solution. *J Alloys Compd* 639:315–324. <https://doi.org/10.1016/j.jallcom.2015.03.052>
14. Narayanan TSNS (2005) Surface pretreatment by phosphate conversion coatings - A review. *Rev Adv Mater Sci* 9:130–177
15. Chauhan LR, Singh M, Singh B, Agarwal AK, Singh SK, Bajpai JK, Misra K (2022) Development of eco-friendly chemical conversion coating for aluminium substrate. *J Indian Chem Soc* 99:100392. <https://doi.org/10.1016/J.JICS.2022.100392>
16. Arun KL, Udhayakumar M, Radhika N (2022) A comprehensive review on various ceramic nanomaterial coatings over metallic substrates: applications, challenges and future trends. *J Bio- Tribo-Corrosion* 9:11. <https://doi.org/10.1007/s40735-022-00717-6>
17. Wang C, Jiang F, Wang F (2004) The characterization and corrosion resistance of cerium chemical conversion coatings for 304 stainless steel. *Corros Sci* 46:75–89. [https://doi.org/10.1016/S0010-938X\(03\)00135-5](https://doi.org/10.1016/S0010-938X(03)00135-5)
18. Zandi Zand R, Verbeken K, Adriaens A (2012) Corrosion resistance performance of cerium doped silica sol-gel coatings on 304L stainless steel. *Prog Org Coat* 75:463–473. <https://doi.org/10.1016/j.porgcoat.2012.06.008>
19. Zuo K, Wang X, Liu W, Zhao Y (2014) Preparation and characterization of Ce-silane-ZrO<sub>2</sub> composite coatings on 1060 aluminum. *Trans Nonferrous Met Soc China* 24:1474–1480. [https://doi.org/10.1016/S1003-6326\(14\)63215-5](https://doi.org/10.1016/S1003-6326(14)63215-5)
20. Xu SA, Wang SN, Gu YY (2019) Microstructure and adhesion properties of cerium conversion coating modified with silane coupling agent on the aluminum foil for lithium ion battery. *Results Phys* 13:102262. <https://doi.org/10.1016/J.RINP.2019.102262>
21. Kong G, Lingyan L, Lu J, Che C, Zhong Z (2011) Corrosion behavior of lanthanum-based conversion coating modified with citric acid on hot dip galvanized steel in aerated 1M NaCl solution. *Corros Sci* 53:1621–1626. <https://doi.org/10.1016/j.corsci.2011.01.038>
22. Hamdy AS, Doench I, Möhwald H (2012) Vanadia-based coatings of self-repairing functionality for advanced magnesium Elektron ZE41 Mg-Zn-rare earth alloy. *Surf Coatings Technol* 206:3686–3692. <https://doi.org/10.1016/j.surfcoat.2012.03.025>
23. Te Tsai Y, Hou KH, Bai CY, Lee JL, Der Ger M (2010) The influence on immersion time of titanium conversion coatings on electrogalvanized steel. *Thin Solid Films* 518:7541–7544. <https://doi.org/10.1016/j.tsf.2010.05.042>
24. Winiarski J, Masalski J, Szczygieł B (2013) Corrosion resistance of chromium-free conversion coatings deposited on electrogalvanized steel from potassium hexafluorotitanate(IV) containing bath. *Surf Coat Technol* 236:252–261. <https://doi.org/10.1016/j.surfcoat.2013.09.056>
25. Chen XM, Li GY, Lian JS (2010) Organic-magnesium complex conversion coating on AZ91D magnesium alloy. *Trans Nonferrous Met Soc China* 20:s643–s647. [https://doi.org/10.1016/S1003-6326\(10\)60554-7](https://doi.org/10.1016/S1003-6326(10)60554-7)
26. Cozzolino R, Segui Y, Raynaud P (2011) Characterization of ZrO<sub>2</sub>/CyHz thin films deposited by MMP-DECR reactor using Zirconium Tert-Butoxide/O<sub>2</sub> mixture. *Surf Coatings Technol* 205:S198–S203. <https://doi.org/10.1016/j.surfcoat.2011.04.085>
27. Tiwari SK, Tripathi M, Singh R (2012) Electrochemical behavior of zirconia based coatings on mild steel prepared by sol-gel method. *Corros Sci* 63:334–341. <https://doi.org/10.1016/j.corsci.2012.06.026>
28. Eivaz Mohammadloo H, Sarabi AA, Sabbagh Alvani AA, Sameie H, Salimi R (2012) Nano-ceramic hexafluorozirconic acid based conversion thin film: Surface characterization and electrochemical study. *Surf Coat Technol* 206:4132–4139. <https://doi.org/10.1016/j.surfcoat.2012.04.009>
29. Samaei A, Chaudhuri S (2022) Role of zirconium conversion coating in corrosion performance of aluminum alloys: An integrated first-principles and multiphysics modeling approach. *Electrochim Acta* 433:141195. <https://doi.org/10.1016/J.ELECTACTA.2022.141195>
30. Chen YW, Moussi J, Drury JL, Wataha JC (2016) Zirconia in biomedical applications. *Expert Rev Med Dev* 13:945–963. <https://doi.org/10.1080/17434440.2016.1230017>
31. Milošev I, Frankel GS (2018) Review—conversion coatings based on zirconium and/or titanium. *J Electrochem Soc* 165:C127–C144. <https://doi.org/10.1149/2.0371803jes>
32. Hamdy AS, Farahat M (2010) Chrome-free zirconia-based protective coatings for magnesium alloys. *Surf Coat Technol* 204:2834–2840. <https://doi.org/10.1016/j.surfcoat.2010.02.063>
33. Eivaz Mohammadloo H, Sarabi AA, Mohammad Hosseini R, Sarayloo M, Sameie H, Salimi R (2014) A comprehensive study of the green hexafluorozirconic acid-based conversion coating. *Prog Org Coat* 77:322–330. <https://doi.org/10.1016/j.porgcoat.2013.10.006>
34. Asemiani HR, Ahmadi P, Sarabi AA, Eivaz Mohammadloo H (2016) Effect of zirconium conversion coating: Adhesion and anti-corrosion properties of epoxy organic coating containing zinc aluminum polyphosphate (ZAPP) pigment on carbon mild steel. *Prog Org Coat* 94:18–27. <https://doi.org/10.1016/j.porgcoat.2016.01.015>
35. Kelly RG, Scully JR, Shoesmith D, Buchheit RG (2002) *Electrochemical Techniques in Corrosion Science and Engineering*. CRC Press, Boca Raton
36. Tait WS (1994) *An Introduction to Electrochemical Corrosion Testing for Practicing Engineers and Scientists*. PairODocs Publications, Racine
37. Liu M, Jin Y, Zhang C, Leygraf C, Wen L (2015) Density-functional theory investigation of Al pitting corrosion in electrolyte containing chloride ions. *Appl Surf Sci* 357:2028–2038. <https://doi.org/10.1016/j.apsusc.2015.09.180>
38. P. Wang, *Corrosion Behaviour of Zirconium Alloys in High Temperature Aqueous Environment By Electrochemical Impedance Spectroscopy*, The University of manchester, 2011
39. Sharifi Golru S, Attar MM, Ramezanzadeh B (2014) Morphological analysis and corrosion performance of zirconium based conversion coating on the aluminum alloy 1050. *J Ind Eng Chem* 24:233–244. <https://doi.org/10.1016/j.jiec.2014.09.036>
40. Awan IZ, A. qadeer Khan, (2018) Corrosion-occurrence and prevention. *J Chem Soc Pakistan* 40:602–655
41. Zhang W, Hurley B, Buchheit RG (2002) Characterization of chromate conversion coating formation and breakdown using electrode arrays. *J Electrochem Soc* 149:B357. <https://doi.org/10.1149/1.1485774>

42. Bond AP, Bolling GF, Domian HA, Biloni H (1966) Microsegregation and the tendency for pitting corrosion in high-purity aluminum. *J Electrochem Soc* 113:773. <https://doi.org/10.1149/1.2424117>
43. Tahamtan S, Fadavi Boostani A (2010) Evaluation of pitting corrosion of thixoformed A356 alloy using a simulation model. *Trans Nonferrous Met Soc China* 20:1702–1706. [https://doi.org/10.1016/S1003-6326\(09\)60361-7](https://doi.org/10.1016/S1003-6326(09)60361-7)
44. Jiao J, Luo Q, Wei X, Qu S, Wang Y, Shen J (2018) Effect of microcracks on the corrosion behavior of Fe-based amorphous coating in chloride solutions. *Int J Electrochem Sci* 13:5522–5534. <https://doi.org/10.20964/2018.06.63>
45. Meunier P, Pirio N, Zirconium & Hafnium, (2011) *Organometallic Chemistry* Based in part on the article *Zirconium & Hafnium: Organometallic Chemistry* by Bernard Gautheron, Roland Brossier, & Philippe Meunier which appeared in the *Encyclopedia of Inorganic Chemistry*. In: Scott RA (ed) *Encyclopedia*. Wiley, Hoboken
46. Van Gorkum R, Bouwman E (2005) The oxidative drying of alkyd paint catalysed by metal complexes. *Coord Chem Rev* 249:1709–1728. <https://doi.org/10.1016/J.CCR.2005.02.002>

**Publisher's Note** Springer Nature remains neutral with regard to jurisdictional claims in published maps and institutional affiliations.

Springer Nature or its licensor (e.g. a society or other partner) holds exclusive rights to this article under a publishing agreement with the author(s) or other rightsholder(s); author self-archiving of the accepted manuscript version of this article is solely governed by the terms of such publishing agreement and applicable law.